Towards Targeted Protein Degradation in *Escherichia coli* - depletion of the essential GroEL protein using CLIPPERs.

Izert-Nowakowska MA[1], Klimecka MM[1], Antosiewicz A[1], Wróblewski K[2], Bandyra KJ[1], Góral TK[3], Kmiecik S[2], Serwa RA[4], Górna MW[1]*

[1] Structural Biology Group, Biological and Chemical Research Centre, Department of Chemistry, University of Warsaw, Warsaw, Poland

[2] Biological and Chemical Research Centre, Faculty of Chemistry, University of Warsaw, Warsaw, Poland

[3] Cryomicroscopy and Electron Diffraction Core Facility, Centre of New Technologies, University of Warsaw, Warsaw, Poland

[4] IMol Polish Academy of Sciences, Warsaw, Poland

Abstract

New, universal tools for targeted protein degradation in bacteria can help to accelerate protein function studies and antimicrobial research. We have created a new method for degrading bacterial proteins using plasmid-encoded degrader peptides which deliver target proteins for degradation by a highly conserved ClpXP protease. We demonstrated the mode-of-action of the degraders on a challenging essential target GroEL. The studies in bacteria were complemented by *in vitro* binding and structural studies. Expression of degrader peptides resulted in a temperature-dependent growth inhibition and depletion of GroEL levels over time. The reduction of GroEL levels was accompanied by dramatic proteome alterations. The presented method offers a new alternative approach for regulating protein levels in bacteria without genomic modifications or tag fusions. Our studies demonstrate that ClpXP is an attractive protease for the future use in bacterial targeted protein degradation.

Introduction

Elimination of the protein of interest by its induced degradation is the state-of-the art approach for studying protein function. While CRISPR technology has revolutionized and facilitated gene knockouts, targeted protein degradation (TPD) tools offer the ultimate progress for interrogating a biological problem: time- and dose-dependent control of protein levels. TPD is also a fast developing area in drug development, in which degrader molecules are used to destroy the target protein involved in pathogenesis. In bacteria, most of the approaches for precise, tunable, and inducible degradation rely on a fusion of the protein of interest with a degron (a degradation signal, often a short sequence motif) [1,2]. Several degron-based systems have been created and used for studying protein function, or used in advanced synthetic biological circuits [3–6]. However, these approaches are only applicable to targets that can be safely tagged without affecting their function, and require genetic modifications which could potentially introduce a bias in the experimental system. Similarly, the use of temperature-sensitive mutants requires genetic modification of the target, and may not be feasible when appropriate mutations cannot be found, or when the studied growth conditions are a limiting factor. Excitingly, the antibiotic pyrazinamide has been found to act by exposure of a native degron in the target protein PanD upon binding of pyrazinoic acid, leading to PanD destabilization and degradation [7]. However, it is difficult to design such destabilizing compounds, so that small-molecule induced instability is not yet a universal mechanism which could be extended to a larger number of bacterial targets. Thus, there is still an unaddressed demand for methods and molecular tools allowing the degradation of native, unmodified bacterial proteins.

In eukaryotic cells, there is a large number of molecular tools for TPD of selected proteins [8]. Such tools include bivalent chimeric molecules such as proteolysis-targeting chimeras (PROTACs) [9], autophagy-targeting chimeras [10], and antibody-based degraders [11,12], as well as monovalent molecular glues [13,14]. These so called degraders have been extensively characterized and they are now entering the clinics [15]. Degraders are attractive drug candidates due to several advantages over conventional inhibitors that must rely on the occupancy of the protein's active site. Degraders allow to target the proteins previously considered as undruggable (such as transcription factors [16] or scaffolding proteins [17,18]). Degraders have been also reported to be effective already in low, substoichiometric concentration due to the distinct event-driven mode of action [19]. Importantly, they act fast enough to decrease the emergence of drug resistance, which has been shown for both cancer and viral targets [20,21].

On many accounts, TPD is therefore a promising approach for creation of new antibiotics, acting through novel mechanisms and with improved properties. However, the conventional TPD approaches exploit protein degradation mechanisms specific for eukaryotic cells (such as ubiquitin-dependent proteasomal degradation or autophagy) and therefore cannot be easily adapted to act in bacteria. Alternatively, direct tethering of proteins to the proteasome was also shown to be an effective strategy for proximity-induced degradation [22]. Previously, we hypothesized that TPD in bacteria might similarly be achieved by direct recruitment of a bacterial protease to the target [2]. Indeed, recently, the first bacteria-specific degraders, BacPROTACs, have been successfully employed to target fusion proteins by tethering them to the mycobacterial ClpC1P protease [23]. These BacPROTACs incorporate the ligand Cyclomarin A specific to ClpC1, a protease component which does not exist in other bacterial phyla beyond Actinobacteria. However, this example gives a premise for creating analogous methods for targeted degradation of endogenous bacterial proteins which could be extended to other bacterial species.

Here, we report a new PROTAC-like approach for degradation of endogenous untagged proteins in *Escherichia coli* using plasmid-encoded Clp-Interacting Peptidic Protein Erasers (CLIPPERs) which directly engage the ubiquitous bacterial ClpXP protease. We demonstrate the effectiveness of the presented method on the example of an essential bacterial chaperone protein GroEL. Our method offers a straight-forward approach for functional studies enabled by selective protein depletion in bacteria. CLIPPERs constitute a starting point towards a new generation of universal bacterial degraders and putative degrader antibiotics acting through the ClpXP pathway.

RESULTS

Establishing a system for peptide-mediated targeted protein degradation in *Escherichia coli*

In search for a universal bacterial TPD system, we embarked first on identifying effective methods for exploiting endogenous proteolytic systems. Since bacteria do not have the canonical ubiquitin-proteasome pathway (and the analogous Pup-proteasome pathway is restricted to Actinobacteria), it is necessary to explore other proteases as the recruited degrading machinery. To create a TPD system in *E. coli*, we have selected a robust protease from the AAA+ family, ClpXP. ClpXP can degrade a number of different substrates [24] but it is mostly known for its involvement in the ribosome-rescue tmRNA (SsrA) pathway, degrading ssrA-tagged polypeptides from stalled ribosomes [25]. The ClpXP system and its interactions with ssrA-tagged substrates and the substrate-delivering adaptor SspB are highly conserved, and they were effectively used for synthetic degron-based systems in a variety of species, both Gram-positive and Gram-negative [26–29]. In the absence of any known suitable small-molecule ClpX ligands, we used peptides interacting with ClpXP to create a new class of degraders: Clp-interacting peptidic protein erasers (CLIPPERs).

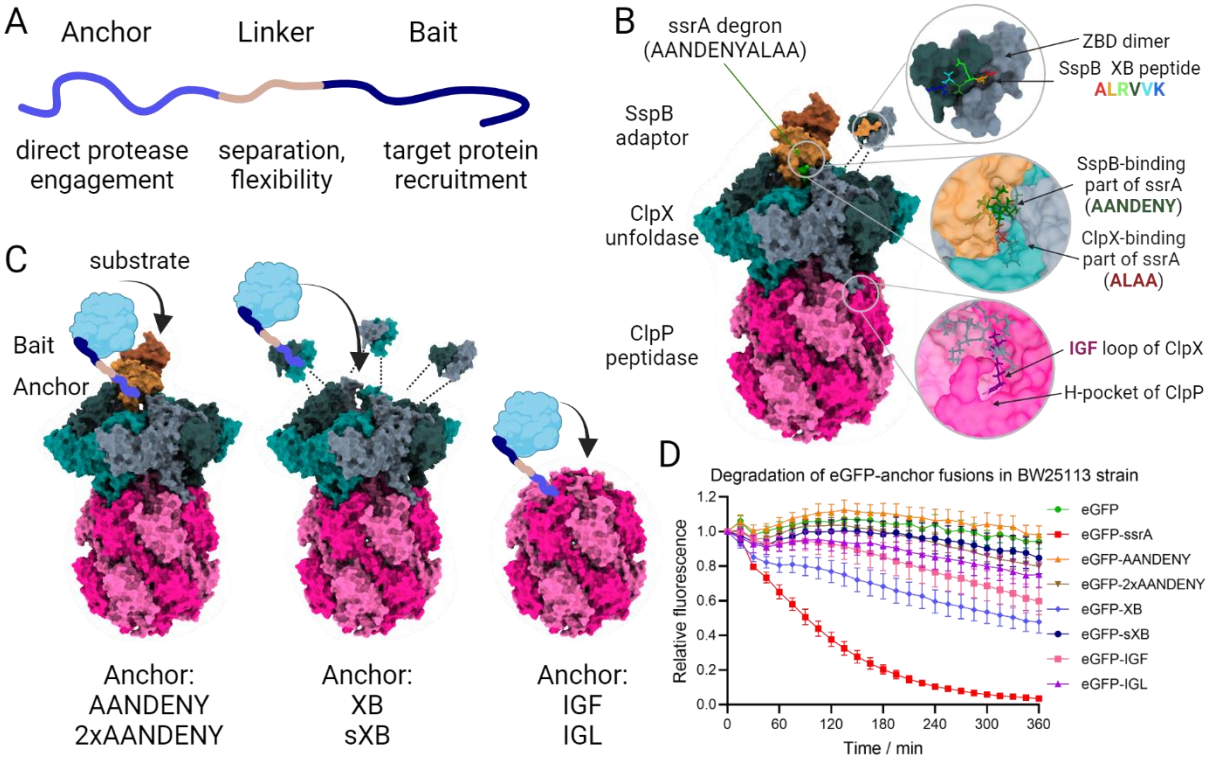

Figure 1. The design of ClpXP-engaging peptidic protein degraders (CLIPPERs)
(A) Schematic representation of the degrader peptides (CLIPPERs). The fusion peptide is composed of an "anchor" which recruits the protease, a "bait" which binds to the target protein and a linker moiety which separates the two peptides. (B) Representation of the ClpXP-SspB complex (based on the ClpXP-SspB-ssrA structure; PDB ID: 8ET3 [30], modified). Indicated are the binding sites of the tested anchor peptides: the SspB-ClpX interface binding the ssrA degron, the Zinc Binding Domain of ClpX with the SspB ClpX-binding peptide (XB), and the IGF loop of ClpX bound in the hydrophobic pocket of ClpP (H-pocket). The C-terminal fragment (XB) of the SspB and ClpX Zinc Binding Domain (ZBD) were not visualized in the experimental structural model and a schematic representation was added based on ZBD-XB crystal structure (PDB ID: 2DS8 [31]). (C) Schematic representation of possible strategies for direct ClpXP recruitment by CLIPPERs binding to SspB, ClpX ZBD, or ClpP. (D) Degradation of the eGFP-anchor fusion proteins in bacteria. The protein levels were monitored by recording bacterial fluorescence following a translation arrest.

CLIPPERs were designed by fusing three different components: an anchor which interacts with the proteolytic machinery, a flexible linker, and a bait which binds to the target protein (Fig. 1A). In order to establish the optimal protease-recruiting strategy, we screened anchors based on known peptides which can interact with either SspB adaptor (the AANDENY fragment of the ssrA degron [32], doubled in the AANDENYAANDENY peptide [33]), ClpX protease (XB and its shorter fragment sXB [31,34]) or directly to the ClpP protease (fragments containing IGF loop from ClpX and IGL loop from ClpA [35]) (Fig. 1B and 1C). The anchors were cloned into the arabinose-inducible expression plasmids at the C-terminus of the eGFP reporter protein. Expression of such fusion constructs in *E. coli* followed by translation arrest resulted in the gradual loss of fluorescence of the eGFP (Fig. 1C). This allowed us to validate the potential anchors which interact with the proteolytic systems and thus could be exploited in TPD approaches. Among the tested anchors the ClpX-binding peptide derived from the C-terminal fragment of the SspB adaptor (XB) was shown to induce a moderate but steady degradation of the fused eGFP. The effect was suppressed in the *clpX*⁻ and *clpP*⁻ *E. coli* mutant strains (Fig. S1A and S1B). We did not observe any effect of the SspB deletion on the XB efficiency (Fig. S1C). The XB-induced degradation was also suppressed in the presence of the protease inhibitor bortezomib (Fig. S2) which confirmed that the loss of fluorescence resulted from proteolysis of the fusion construct. Although eGFP-ssrA fusion resulted in the most efficient degradation, the ssrA peptide is engaged directly in the entry pore of ClpX and thus ssrA-

based CLIPPERs would be highly susceptible to degradation themselves. Moreover, even if such “suicidal” ssrA-based CLIPPERs would be efficient, the location of ssrA degron must be C-terminal for recognition by ClpX, which would limit possible peptide order in CLIPPER design to using only N-terminal baits. In contrast, the XB peptide is engaged by the dimeric Zinc Binding Domain of ClpX regardless of XB motif position in the polypeptide, and might reduce CLIPPER proteolysis while still inducing efficient proximity-based degradation of the target. The XB peptide was therefore selected as the leading candidate for use as the CLIPPER anchor in our peptide-based TPD.

Peptide-mediated GroEL depletion dysregulates bacterial proteostasis

To test whether CLIPPERs containing the XB fragment could be used for depleting endogenous proteins in bacteria, we have designed fusion peptides composed of an N-terminal Myc peptide tag, followed by the XB anchor, a flexible linker and a bait peptide. Although peptides can be potentially used as antimicrobials, their effective import in bacteria can present challenges that are yet to be addressed [36,37]. To omit such limitations, we have created a series of arabinose-inducible expression plasmids encoding the tested fusion peptides to study the effect of CLIPPER expression on bacterial phenotypes. To demonstrate the mode of action of the peptide degraders, we have chosen the GroEL chaperone as a potential TPD target. GroEL is conditionally essential in *E. coli* which enables a facile phenotypic readout of the GroEL protein loss in cells. GroEL is known to assist the folding process of multiple proteins and many of them depend strictly on the GroEL [38–40]. GroEL was identified as a potential antimicrobial target although currently there are no GroEL-targeting therapeutics in use [41,42]. Targeting an essential protein which regulates multiple other proteins appeared to be an attractive strategy to observe the phenotype changes even in case of moderate degradation of the target. Additionally, GroEL has a well-defined peptide ligand, the “strong binding peptide” (SBP) [43], which binds to GroEL without disrupting its activity. Our preliminary experiments for degraders of another *E. coli* chaperone DnaK exploiting its known peptide ligands [44,45], have demonstrated that using highly toxic baits as a part of degrader constructs can make it difficult to distinguish the effect of the bait from the degradation event (Fig. S3 A and S3 B). Thus, targeting GroEL with the relatively non-toxic SBP peptide appeared as a suitable approach for demonstrating the action of CLIPPERs.

To verify whether GroEL-targeting CLIPPERs (GroTAC1 and GroTAC2, including flexible GGS and GGSGGSGG linkers, respectively; Fig.2A) can affect bacterial growth, we have assessed *E. coli* growth in the presence or absence of the expression-inducing arabinose. The initial screening showed that expression of GroTACs can impair the growth of bacterial colonies in a temperature-dependent manner (Fig. 2B). We did not observe any effect of either the XB anchor or the SBP bait on bacterial growth. The initial results were confirmed by experiments in liquid cultures. The expression of GroTACs with two different linker lengths resulted in moderate growth inhibition reaching around 20-25% when bacteria were cultured at a permissive temperature of 30°C (Fig. 2C). The effect was not observed in the *clpP*- mutant strain (Fig. S4). The observed reduction was potentiated when bacteria were cultured at an elevated temperature of 42°C, when proteins are more prone to misfolding and the folding activity of GroEL is more essential (Fig. 2D). The observed growth reduction depended on the level of peptide expression (Fig. 2E), although the regulation of pBAD vectors do not display linear response to inducer concentration [46]. The changes in bacterial growth observed by monitoring cell culture density were confirmed with an enzymatic viability assay (Fig. 2F). The expression of the degraders in 42 °C caused a significant reduction in *E. coli* viability which was even greater than the reduction in culture density. This allowed us to conclude that the tested GroTACs influence bacterial fitness in thermal stress. To test whether the observed differences are caused by alterations in the GroEL levels, we have performed a western blot analysis at several different time points after the induction of bacteria cultured at 42 °C. We observed the consequent decrease in the GroEL protein level in bacteria expressing GroTACs in comparison to bacteria expressing the control peptides (Fig. 2G and S5). The reduction

reached up to 40% of the GroEL level in comparison to the control groups which was in agreement with the viability experiments. Additionally, visualization of the whole protein content on the membranes by a stain-free technique revealed dramatic alterations in the protein pattern in GroTAC-expressing bacteria (Fig. S5). The alterations and the apparent loss of proteins was observed regardless of the normalization strategy (normalization to the protein content or the number of bacterial cells). This suggested that even modest loss of GroEL can have a dramatic effect on the bacterial proteome.

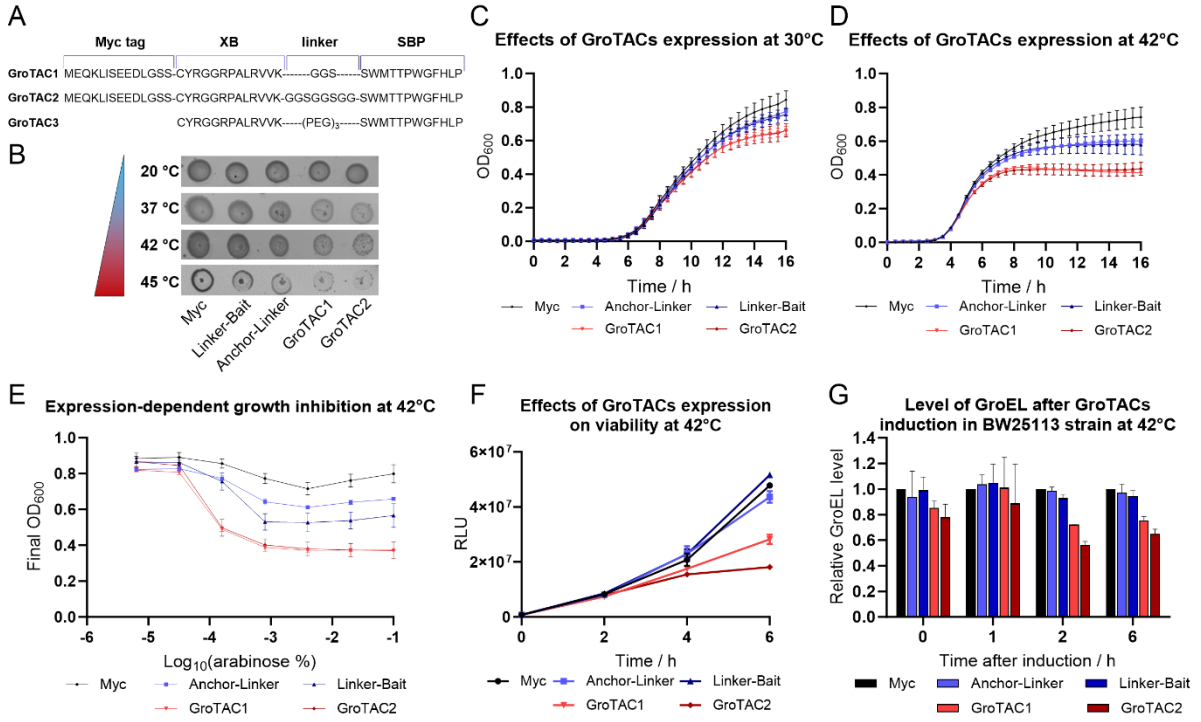

Figure 2. *E. coli* BW25113 bearing plasmids with tested peptides (Myc control peptide, anchor-linker, linker-bait and GroTACs with two linker lengths) were subjected to growth tests and GroEL levels measurement. (A) A schematic of the composition of the GroTAC peptides. (B) Drop test of bacteria grown on LB plates with 0.02% arabinose incubated at different temperatures. (C) Growth curves of bacteria grown at 30 °C in the presence of 0.02% arabinose. (D) Growth curves of bacteria grown at 42 °C in presence of 0.02% arabinose. (E) The effect of arabinose concentration on bacterial growth at 42 °C. (F) Enzymatic viability test of bacteria at different time points after induction of peptide expression at 42 °C. (G) Western blot measurement of GroEL level at different time points after induction of peptide expression; representative blots and quantified results normalized to the level of GroEL in bacteria expressing Myc peptide.

To verify how the GroEL depletion affected the levels of other proteins, we have performed a quantitative shotgun proteomics analysis of the bacterial proteomes at 1 hour (Fig. 3A and D), 2 hours (Fig. 3B-E) and 6 hours (Fig. 3C-F) after induction of peptide expression in *E. coli* grown at 42°C. We identified 2357 protein groups matched to the reference proteome, including 1857 consistently quantified across all replicates and experimental conditions. We also identified a tryptic peptide LISEEDLGSSCYR originated from the XB motif of the GroTACs, providing additional evidence for their reproducible expression under the chosen experimental conditions. The analysis revealed that GroTAC expression results in a progressive dysregulation of the bacterial proteome with hundreds of proteins up- or downregulated, which was not observed in the bacteria expressing the control peptides (Fig. S6). After 6 hours expression of the Linker-Bait peptide we have observed a decrease in levels of several proteins which suggests that the Anchor peptide itself might possibly interfere with cellular functions of GroEL. The MS results confirmed the GroTAC-induced progressive reduction of the GroEL level observed during western blot experiments (Fig. 3G). Among changed proteins, besides GroEL, we have observed the progressive downregulation of the obligate GroEL substrates, known as class IV substrates [39] (Fig. 3(A-F); Fig. S7). Other classes

of substrates can either fold spontaneously or be assisted by other bacterial chaperones [38,39], thus we did not observe significant overall changes in their relative levels. The downregulation of obligate substrates was not observed at 1 hour but appeared at 2 hours and was even more pronounced at 6 hours after induction, which may point to a secondary effect of the GroEL depletion that needs time to develop. Even partial GroEL depletion can thus affect the level of its clients presumably by impairing their folding which can lead to aggregation or proteolytic degradation. The downregulation of GroEL was accompanied by changes in levels of a number of other proteins involved in regulating cellular proteostasis (Fig. 3H). We observed that the GroEL-interacting co-chaperonins GroES and CnoX (YbbN) were also downregulated in GroTAC-expressing bacteria. The reduction in their levels could be an additional effect of the induced proximity between GroEL and ClpXP, which in principle could facilitate degradation of target-bound proteins. Several other chaperones were altered including downregulated DnaK, GrpE, HptG and ClpB. At the same time, another chaperone, trigger factor (TF), was significantly upregulated together with its substrates, ribosomal proteins [47] (Fig. S7). This could indicate an activation of a rescue mechanism to compensate for the loss of GroEL. We also observed changes in the level of several proteins involved in proteolysis such as Lon, DegP, and ClpP with its partners ClpA, ClpX, and ClpS. This suggests that the GroTAC-mediated GroEL depletion can induce massive alterations to the cell proteostasis, which in thermal stress result in severe growth dysfunctions and cell death. Since GroEL is interacting with hundreds of protein partners involved in a variety of processes, even its incomplete depletion has severe effects on the bacterial proteostasis.

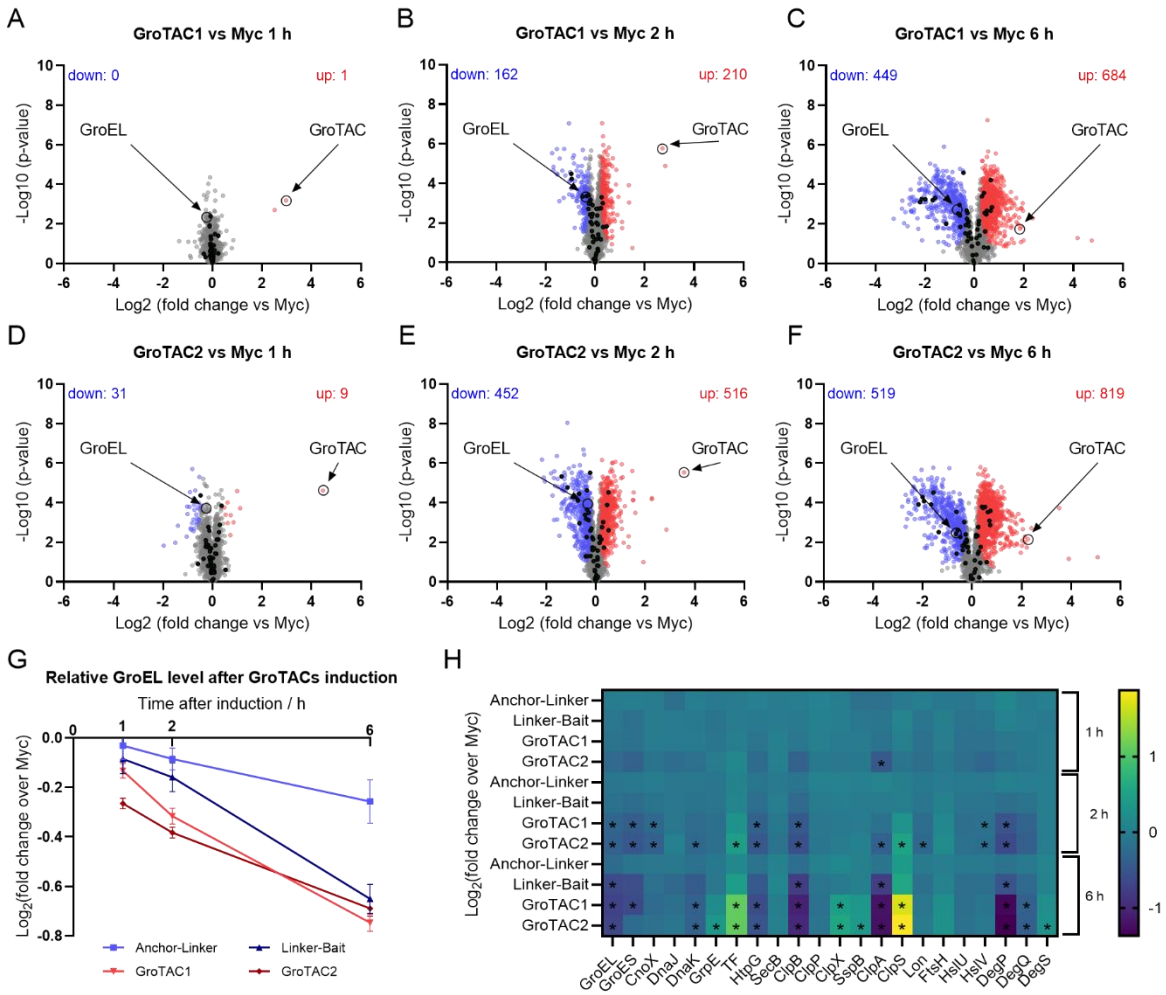

Figure 3. Proteomics analysis of *E. coli* BW25113 expressing GroTACs. (A) – (F) Volcano plots displaying the log2 fold change (log2FC, x axis) against the t-test-derived −log10 statistical

p-value (y axis) for protein groups detected in total lysates of *E.coli* expressing GroTAC1 or GroTAC2 for 1h (A and D, respectively), 2h (B and E, respectively), and 6h (C and F, respectively) compared to *E.coli* expressing control peptide, Myc, by LC-MS/MS analysis (n = 3). Student's t-test (two-sided, unpaired) was performed for the statistical analysis. Proteins levels found upregulated, downregulated, and unchanged are indicated as red, blue, and gray dots, respectively. The obligate GroEL substrates are marked with black dots. GroEL and GroTAC are marked with open circles. (G) Relative changes in GroEL levels in bacteria expressing GroTACs and control peptides. (H) Heat map representation of changes in levels of proteins involved in cellular proteostasis, statistically significant changes (q-val < 0.05) are marked with asterisks.

In vitro validation of GroTAC action suggests the mechanistic limitations of CLIPPERs

In order to validate the mode of action of the GroTACs we performed a series of *in vitro* experiments using purified peptides and proteins. The first prerequisite of the GroTACs action is binding to its protein partners ClpX and GroEL. We have assessed the binary interactions of His-SUMO-tagged GroTACs or their components with their respective partners by biolayer interferometry (BLI) (Fig. 4, Table S1). The isolated ClpX was binding to the XB-GGS (anchor-linker) peptide with 65 nM affinity (Fig. 4A). The GroTAC1 peptide had a similar affinity towards ClpX (70 nM) suggesting that the XB peptide retains its binding capacity even in fusion with other peptides. The binding event alone might not be sufficient to cause the ClpXP-mediated degradation of tethered target proteins. It is known that the SspB adaptor activates the ClpXP complex by stimulating its ATPase activity and the XB peptide alone can also activate ClpX. We have tested if GroTAC1 retains similar ClpX-activating properties. To our surprise GroTAC1 displayed even more potent stimulation of the ClpX ATPase activity than the XB-GGS peptide alone even though the GGS-SBP peptide had no effect on the ClpX (Fig. 4C, Table S1). Therefore, GroTAC1 not only binds but also activates ClpX which increases its degrading potential. GroEL was bound by GGS-SBP (linker-bait) with an affinity of 94 nM (Fig. 4D). GroTAC1 had moderately reduced affinity towards the GroEL (154 nM), however the binding was still in the similar nanomolar range (Fig. 4E). At the same time we observed a significant deviation from the 1:1 binding stoichiometry which could suggest uneven occupancy of the SBP-binding sites of the GroEL subunits, however this could also arise from steric constraints (only one side of the GroEL barrel can face the peptide-covered sensor surface). This leads to the conclusion that fusion of the XB anchor with the SBP bait did not perturb significantly the interactions between these peptide fragments with their respective protein partners and that GroTAC1 retains the binding capacities similar to the individual peptide ligands. Next, we attempted to reconstitute the protease system to verify if we can observe the degradation *in vitro* using purified peptides and proteins: ClpXP complex, GroTAC1 and GroEL. In the tested conditions we only observed a modest degradation of the GroEL reaching around 40% after 10 hours incubation in a reaction mixture (Fig. 4F).

To better understand the binding topology between GroTAC and GroEL we obtained a structural model of their complex using cryogenic electron microscopy. The obtained electrostatic potential map revealed an additional volume at the top of the GroEL barrel lumen, in the area of the GroEL apical domain. This is in concert with the binding site of the SBP peptide in the crystal structure of GroEL in complex with SBP (PDB ID 1MNF) (Fig. 4G). The low resolution of our experimental map in this region might be due to reduced occupancy and/or flexibility of the GroTAC3 molecule. The additional density attributed to the ligand corresponded to the size and orientation of SBP in the available co-crystal structure. *Ab initio* modelling tools such as AlphaFold or ModelAngelo consistently indicated the presence of a proline in the position corresponding to the middle of the SBP peptide in the crystal structure (Fig. 4G). We managed to model the SBP part of GroTAC3 into the corresponding electrostatic potential density based on the tracing of peptide backbone and the positioning of P22 in the middle of SBP. Thus, the results confirmed unambiguously that GroTAC can effectively bind to the GroEL target. However, the XB-linker segment of GroTAC could not be visualised due to extremely low resolution – this suggests the expected high flexibility and mobility of the unbound rest of the GroTAC in the absence of ClpX.

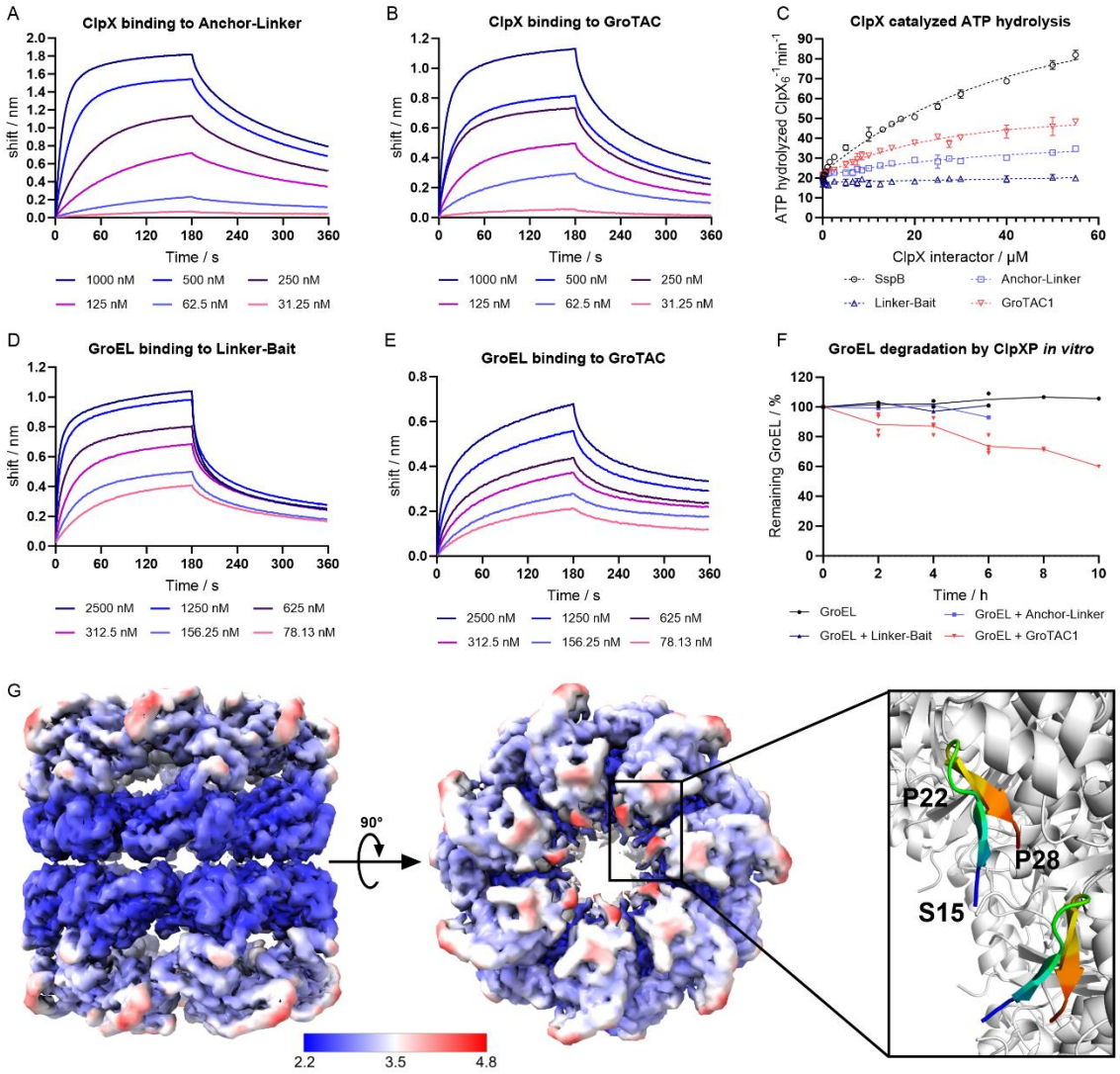

Figure 4. *In vitro* analysis of GroTACs interactions with ClpX and GroEL.

(A) Sensograms representing the BLI measurement of ClpX binding to His-SUMO-XB-GGS peptide; (B) Sensograms representing the BLI measurement of ClpX binding to His-SUMO-GroTAC1 peptide. (C) Stimulation of ATPase activity by a natural ClpX partner (SspB) and the peptides used in the study. (D) Sensograms representing the BLI measurement of GroEL binding to XB-GGS peptide. (E) Sensograms representing the BLI measurement of GroEL binding to GroTAC peptide. (F) *In vitro* degradation of GroEL by ClpXP in presence of tested peptides. (G) Electrostatic potential density map obtained by CryoEM, coloured by local resolution, and visualization of GroTAC3 molecules (rainbow) binding to GroEL subunits based on the obtained structure from CryoEM map.

Discussion

Modification of protein stability by specific peptidic degrons, such as ssrA, is a well-established strategy which has been used for studying protein function [2]. A common inducible degradation system relies on constitutive expression of an ssrA-tagged protein of interest and inducible expression of SspB adaptor [48]. However, studying protein function in the *sspB*- genetic background, when protein turnover can be reduced, might introduce some bias. Additionally, this approach requires genetic modifications (i.e. creating fusions) of target proteins in bacteria. Introducing tags can alter protein folding, activity, or localization [49–51]. For example, in our hands, purified GroEL fused with a purification tag could not be assembled into functional barrels. Here, we propose a novel method for inducible, peptide-mediated depletion of native, unmodified, endogenous bacterial proteins.

We used the SspB-derived “XB” peptide which binds and activates the ClpX component of the bacterial ClpXP proteolytic complex. The interactions between SspB and ClpX are highly conserved, so that heterologously expressed SspB can interact with ClpX of bacteria normally lacking this adaptor [26,27]. This gives a premise of the wide universality of the proposed approach. The XB peptide has been used before as a FKBP12-XB fusion for rapamycin-inducible degradation of ssrA-tagged proteins using a split SspB adaptor system [29]. This has substantiated our further premise that induced proximity by tethering to ClpXP would be sufficient for engineering bacterial TPD, though a degron-less target has not been previously attempted. In our study we used the XB peptide in CLIPPERs in direct fusion with a target-interacting peptide to cause degradation of unmodified endogenous proteins. This shows that tethering the native target protein to the activated ClpXP protease complex can induce the target degradation. Such an effect has been previously demonstrated in the recent pioneer works on bacterial small-molecule degraders (BacPROTACs) exploiting the ClpCP protease in Mycobacteria and Gram-positive bacteria [23,52]. BacPROTACs hold high promise as an exciting novel type of antibiotics that relies on a completely different mechanism of action from classical inhibitors. Expanding the spectrum of TPD repertoire against more bacterial orders is of critical importance in future antibiotic development. The most lethal antimicrobial-resistant pathogens are predominantly Gram-negative species [53] which do not express ClpCP, and thus cannot be targeted by the currently known BacPROTACs. Our work opens the doors to TPD based on a ClpP protease also in Gram-negative bacteria and suggests that the ClpX-XB interactions might be worth exploring for future design of specific ClpX-binding small molecules for potential use in new BacPROTACs.

We demonstrated the use of our new method on an essential bacterial chaperone GroEL, which is a potential antimicrobial target [41,42]. Using a well-characterized peptidic ligand of GroEL (SBP) as the bait in an XB-based CLIPPER resulted in progressive loss of GroEL upon CLIPPER expression. This approach has been efficient already at 1 h post-induction and against a high-copy target such as GroEL, present in cells at more than 1 order of magnitude higher protein levels than ClpXP itself [54,55], while the concentration of GroEL increases further up to 10-fold at high temperatures. A model GFP-ssrA substrate was reported to be degraded by the cellular ClpXP pool at a rate of 100 000 molecules per generation in *E. coli* cells doubling every 20 min [55]. In our hands, GroTAC2 expression reduced GroEL protein level by ~17% in 1 h in cells growing at 42°C. Even considering fast synthesis of new GroEL copies (~50 000 – 60 000 molecules per cell generation [56]) which may obfuscate the real *in vivo* degradation rate, this result still suggests that a native degron-less protein is indeed a markedly more difficult target for the tethering-induced degradation than the typical ssrA-tagged substrates. This difference might be due to slower initiation of degradation, since unstructured terminal tags might more readily engage the protease pore. However, even moderate GroEL depletion resulted in decreased bacterial survival and dysregulation of the *E. coli* proteome. This is consistent with GroEL function as a central hub in maintaining bacterial proteostasis in environmental stress. CLIPPER-mediated protein downregulation can therefore be used to study the function of proteins of interest, or to validate antibiotic targets, advantageously also in a time-resolved manner and in case of essential proteins or those not amenable to tagging. Since CLIPPER design was relatively straightforward and modular, we expect it can be easily extended to other targets using their known interacting peptides as baits.

Our study also reveals some of the limitations and requirements of using TPD in bacteria, and poses further questions. We hypothesize that the highly stable and well-ordered GroEL barrels could be naturally resistant to degradation by ClpXP. We suspect that the degradation can only occur for a fraction of dissociated, monomeric GroEL which justifies the limited degradation observed both *in vitro* and in bacteria. Higher temperatures destabilize the GroEL complexes [57] and stimulate the expression of GroEL [58]. We suspect that in bacteria we observe predominantly GroTAC-mediated degradation of newly translated unassembled GroEL subunits, which could be easier to engage and deliver to ClpXP (Fig. 5). A similar phenomenon

was recently shown for human chaperones which are resistant to degradation in their assembled state, but recognized by their cognate adaptors and delivered for ubiquitination in the free, monomeric state [59,60]. This could also suggest that other than target protein half-life, which is a known factor limiting TPD efficiency of degraders acting in human cells (i.e. depletion of short-lived targets has less of a marked effect [61]), in bacteria also the synthesis rates would be critical, and those might alter more widely in prokaryotes depending on environmental stimuli. GroEL synthesis rate is high in normal conditions (~52 000 copies per generation [56]), which might have facilitated GroTAC action by promoting access to unassembled subunits. On the other hand, targets with a high protein copy number might also be more resistant to TPD approach, depending on how well the target protein pool can buffer the demand for its function - though due to fitness requirements, bacteria might have optimized the protein synthesis burden [56] leaving little redundancy in some cases, as might have been the case of GroEL. Exploiting conditions which increase the demand for the target (such as elevated temperatures for GroEL) can help identify the most efficacious TPD applications.

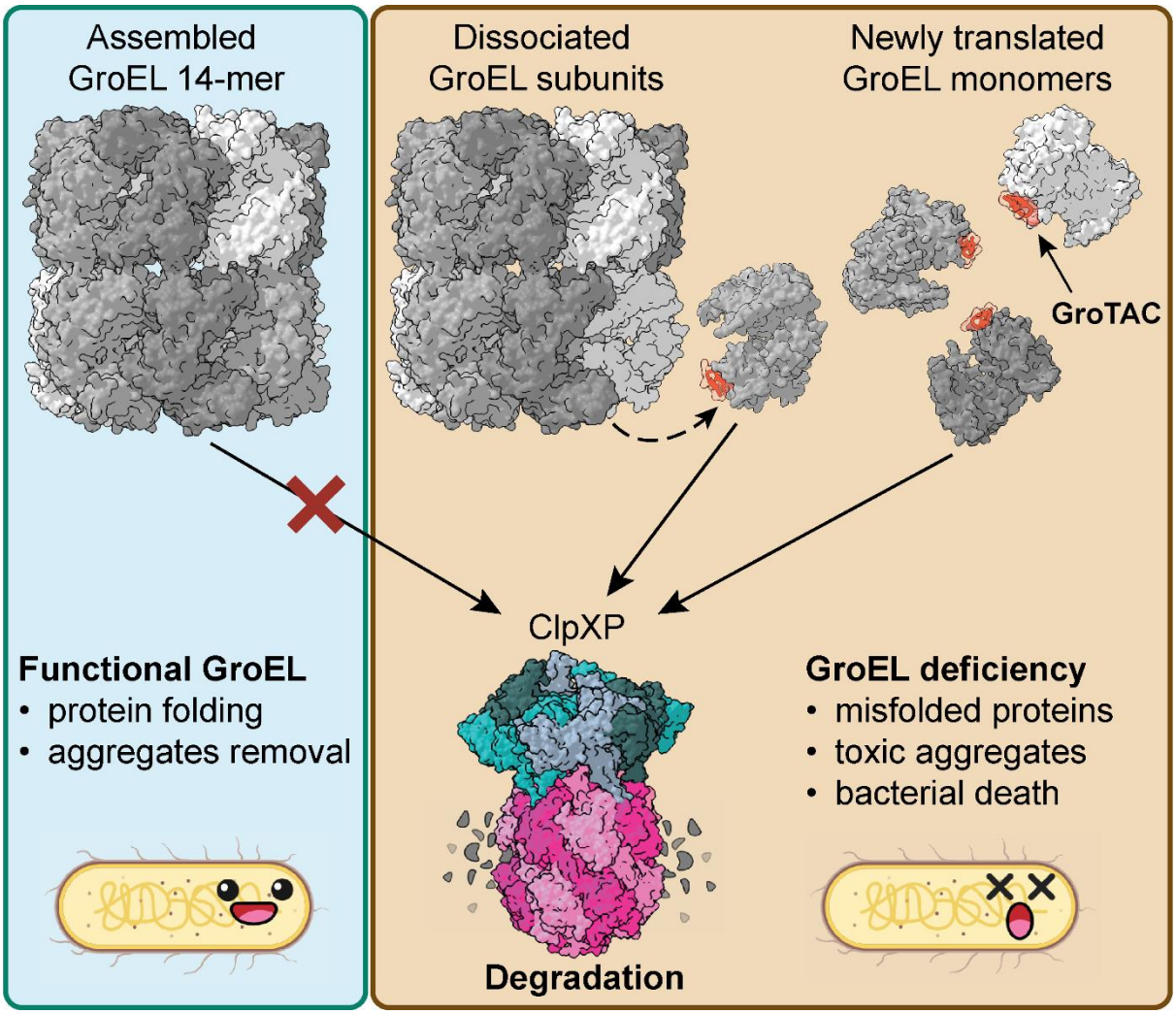

Fig. 5 Schematic representation of GroTACs mode of action

Several other protein targets could not be degraded in our hands using other tested CLIPPER prototypes which suggests that the range of proteins prone to CLIPPER-mediated degradation might be limited and/or their degradation could depend on specific culture conditions. A number of inherent factors can determine protein stability and susceptibility to proteolysis. For instance, although ClpXP can extract tagged proteins from the membranes [62] or protein complexes [63], the effectiveness of degradation of membrane proteins depends on protein topology and accessibility [64]. Similarly, protein fold determines the degradation potency since ClpXP

engages its substrates by either N or C-terminus [24]. Both N- and C-terminus of GroEL are facing the interior of the GroEL barrel which makes it difficult to engage without prior disassembly of the multimer. It was shown that the small-molecule BacPROTACs induce target degradation with different potency, depending on the substrate fold, with preference toward unstructured proteins [23]. Thus, the potency of the degraders which directly engage proteases is not universal towards all targets. The presented method exploiting plasmid-expressed CLIPPER peptides seems to be best suited for less structured, monomeric, and cytoplasmic proteins. Lastly, identifying baits with sufficient binding affinity might also play a role in extending applications of the CLIPPER technology to further targets. Here, either prior knowledge of interacting peptides would be necessary, or bait peptides might be developed through experimental methods such as phage display, as was done for SBP and GroEL. Advantageously, as compared to inhibitors, TPD approaches allow to explore more potential binding pockets in the protein. CLIPPERs obviate the requirement for targeting the active site, and thus extend the target range to non-enzymes including many cases considered classically "undruggable". However, the limitation to ligandable targets remains, as good and specific binding is still the TPD prerequisite. Fortunately, peptides are considered a relatively easier way to develop good binding properties due to their typically larger interaction surfaces than small molecules. All of the above might entice researchers to try CLIPPERs in the first instance as useful tools, on their way to developing more drug-like TPD agents based on small molecules that may have better chances of penetrating into the bacteria. Finally, future research developments might perhaps also find ways of efficient peptide delivery to bacterial cytoplasm, which would overcome the ultimate limitation of CLIPPERs as titratable TPD tools and drugs.

Here, we achieved the first demonstration of a designed TPD-like approach acting on an unmodified target protein in a model Gram-negative bacterium. CLIPPERs present a new way to control protein function by degradation, which can enable functional studies of bacterial proteins or may find applications in biotechnology and synthetic biology. Our method also constitutes a new tool for validation of drug targets, and especially might assist assessing conditions and target suitability and degradability in the potential development of new bacterial degraders. The eventual replacement of peptides with small molecules would be a promising strategy for creating next-generation ClpXP-engaging bacterial degraders which could be applied in a variety of bacterial species including the most threatening Gram-negative pathogens.

Materials and Methods

Cloning

The complete list of DNA constructs and primers used in this study is provided in Table S2.

The pBAD-eGFP (here referred to as pBAD-6xHis-TEV-eGFP) vector was a gift from Michael Davidson (Addgene plasmid # 54762 ; http://n2t.net/addgene:54762 ; RRID:Addgene_54762). The pBAD-6xHis-TEV and pBAD-6xHis-TEV-eGFP-peptide were obtained by site directed mutagenesis of pBAD-eGFP [33]. The constructs encoding Myc-degrader fusion peptides were obtained by multistep site-directed mutagenesis by substitution of 6xHis-TEV sequence of pBAD-6xHis-TEV-eGFP with Myc tag and then introducing the degrader-encoding sequence in place of eGFP. The plasmids were amplified by PCR with primers introducing the mutations. The purified products were subjected to phosphorylation and ligation and the obtained constructs were transformed into *E. coli* Top10 for selection on Ampicillin.

The preparation of constructs for protease purification (pET28a-6xHis-SUMO-ClpP, pET28a-6xHis-SUMO-SspB, pBAD-6xHis-SUMO-ClpX) was described before [33].

The construct for GroEL purification was obtained by SLIC cloning of GroEL gene amplified from *E. coli* BW25113 DNA into pET28a-6xHis-SUMO vector followed by transformation to *E. coli* Top 10 for selection on Kanamycin. The obtained pET28a-6xHis-SUMO-GroEL was then subjected to 6xHis-SUMO deletion by site-directed mutagenesis as described above to obtain the untagged pET28a-GroEL construct and transformed into *E. coli* Top10 for selection on Kanamycin.

The constructs for peptide purification were obtained by annealing peptide-encoding DNA oligomers, digestion with BamHI and XhoI restriction enzymes, and ligation with digested and purified pET28a-6xHis-SUMO vector followed by transformation to *E. coli* Top10 and selection on Kanamycin.

The list of the plasmids with respective oligonucleotides used for cloning is provided in Table S3. The list of *E. coli* strains used in the study is provided in Table S4.

Protein purification

ClpP, ClpX, SspB and eGFP-ssrA were purified as described before [33].

Overexpression of untagged GroEL and peptides was carried out in *E. coli* C43 DE3 and BL21 DE3 strains, respectively. Protein expression was induced at OD_{600} ~0,6-0,7 with 1 mM IPTG. After 3 h at 30 °C (GroEL) or 16 h at 18 °C (peptides) cultures were centrifuged (5180 xg, 30 min, 4°C) and bacterial pellets were collected and frozen at -20°C.

Bacterial pellet containing untagged GroEL was lysed in the buffer containing 20 mM Tris pH 7.5, 10 mM NaCl, 10 mM $MgCl_2$, 1 mM EDTA, 1 mM DTT with addition of lysozyme (100 mg) and DNase (20 U). After 30 min at 4 °C, the lysate was sonicated (15 min, 45 on / 15 off sec, 40% amplitude at 4 °C) and centrifuged (48380 xg, 30 min, 4 °C). Next, lysate was cleared by filtration (0.8 um) and applied on the HiTrapQ, 5ml column (Cytiva). After washing, the column was eluted with a lysis buffer with 1 M NaCl. Fractions containing GroEL identified by SDS-PAGE were combined and then concentrated in Amicon Ultra-15, 30K MWCO (Merck Millipore) (5000 xg at 4°C). Then, a sample with addition of 5 mM ATP was applied on a Superdex200 10/300 column (Cytiva) using 50 mM Tris pH 7.5, 150 mM NaCl, 1 mM EDTA, 1 mM DTT, 20% EtOH. Quality of eluted GroEL was assessed on SDS-PAGE and proper fractions were combined and concentrated in Vivaspin 6, 30K MWCO (Sartorius) (8000 xg at 4 °C) with a buffer change to 50 mM Tris pH 7.5, 150 mM NaCl, 1 mM DTT, 2.5 mM ATP. GroEL concentration was measured at 280 nm and it was stored at -20 °C.

Bacterial pellets after peptides overexpression were lysed in the buffer containing 25 mM Tris pH 7.5, 300 mM NaCl, 20 mM imidazole, 1 mM DTT with addition of lysozyme (100 mg) and DNase (20 U). After 30 min at 4 °C, the lysates were sonicated (15 min, 45 s on / 15 s off, 40% amplitude at 4 °C) and centrifuged (48380 xg, 30 min, 4 °C). Next, the lysates were cleared by filtration (0.8 µm) and applied on the on HisTrap, 5 ml column (Cytiva). After washing, the column was eluted with a lysis buffer containing 500 mM imidazole. Presence of peptides was confirmed by SDS-PAGE and proper fractions were combined and dialysed to buffer containing 25 mM Hepes pH 8,0, 300 mM NaCl, 1 mM DTT. After 2 h at 4°C with one change of buffer peptides were concentrated in Vivaspin 500, 10K MWCO (Sartorius) (10000 xg at 4 °C) and their concentration was measured at 280 nm. Finally peptides were flash frozen in liquid nitrogen and stored at -80 °C.

eGFP degradation in bacteria

The degradation of eGFP-peptide constructs in bacteria was performed as described before [33] with minor modifications. Overnight cultures of *E. coli* BW25113 or mutant strains [65] carrying plasmids: pBAD-6xHis-TEV, pBAD-6xHis-TEV-eGFP, pBAD-6xHis-TEV-eGFP-ssrA, pBAD-

6xHis-TEV-eGFP-AANDENY, pBAD-6xHis-TEV-eGFP-2xAANDENY, pBAD-6xHis-TEV-eGFP-XB, and pBAD-6xHis-TEV-eGFP-sXB were grown in LB medium supplemented with Ampicillin (100 µg/ml) at 37 °C with shaking. The cultures were then diluted 1:100 in 5 ml of fresh LB with Ampicillin (100 µg/ml) and grown to mid-exponential phase (OD_{600} 0.5 – 0.6). The expression of plasmids was induced by addition of L-arabinose to the final concentration of 0.005% and the bacteria were further cultured overnight at 18 °C. The cultures were then diluted 1:20 in a 96-well microplate in 200 µl of M9 medium supplemented with Ampicillin (100 µg/ml), Spectinomycin (100 µg/ml) and 0.2% glucose (to arrest the expression of protein constructs). The degradation was then monitored by measuring OD_{600} and fluorescence (excitation at λ = 489 nm and emission at λ = 520 nm). The measurements were taken every 15 minutes for 6 h at 30 °C with shaking in between measurements in Tecan Infinite M200 Pro plate reader. The fluorescence was normalized to the optical density and the background of bacteria expressing the control pBAD-6xHis-TEV vector was subtracted. The values at 0 time point were set as 100%.

The bortezomib inhibition assay was performed likewise, except that after the overnight induction the bacterial cultures were diluted in the antibiotics-supplemented M9 medium with the addition of 1% DMSO or Bortezomib in DMSO in concentrations 10 µM, 50 µM, 100 µM, 250 µM or 500 µM.

Serial dilution plate test

Overnight cultures of *E. coli* BW25113 strains transformed with pBAD plasmids encoding degraders and control peptides were grown in LB medium with Ampicillin (100 µg/ml). The cultures' OD_{600} was measured and normalized to 1.0. The cultures were then serially diluted in sterile PBS in final concentrations from 10-1 to 10-6. The 2 µl drops of the dilutions were put on LB agar with Ampicillin and with or without 0.02% L-arabinose. The plates were then incubated in appropriate temperatures overnight (for temperatures 37 °C and above) or up to 36 h (for lower temperatures).

Bacterial growth measurement

Overnight cultures of *E. coli* BW25113 or mutant strains transformed with pBAD plasmids encoding degraders and control peptides were grown in LB medium with Ampicillin (100 µg/ml) and in case of mutant strains also Kanamycin (30 µg/ml). The cultures were then diluted 1:50 000 in a 96-well microplate in 200 µl of LB supplemented with appropriate antibiotics and with or without addition of 0.02% L-arabinose. The cell growth was then monitored by measuring OD_{600}. The measurements were taken every 30 minutes for 16 h at either 30 °C or 42 °C with shaking in between measurements in Tecan Infinite M200 Pro plate reader. The dose-response experiments were performed likewise, except the 5-fold dilutions of arabinose were used, ranging from 0.1% to $6.4e^{-6}$ %.

Measuring bacterial viability with BacTiter-Glo

Overnight cultures of *E. coli* BW25113 strains transformed with pBAD plasmids encoding degraders and control peptides were grown in LB medium with Ampicillin (100 µg/ml). The cultures were then diluted 1:100 in 10 ml of fresh LB with Ampicillin and grown at 37 °C to OD_{600} 0.1-0.2. The cultures were then induced with 0.02% L-arabinose and grown at 30 °C or 42 °C with shaking. The OD_{600} and bacterial viability measurements were taken at 0, 2, 4 and 6 h post-induction. The bacterial viability was measured using luminescence-based BacTiter-Glo Microbial Viability Assay (Promega) according to the manufacturer's protocol. The luminescence measurements were taken in Tecan Infinite M200 Pro plate reader.

Western blot

Overnight cultures of *E. coli* BW25113 strains transformed with pBAD plasmids encoding degraders and control peptides were grown in LB medium with Ampicillin (100 µg/ml). The cultures were then diluted 1:100 in 10 ml of fresh LB with Ampicillin and grown in 37 °C to OD_{600} 0.1-0.2. The cultures were then induced with 0.02% L-arabinose and the temperature was shifted to 42 °C. The samples corresponding to OD_{600}=0.2 were collected at 0, 1, 2 and 6 h after induction. The culture aliquots were centrifuged for 5 min at 2 000 xg in 4 °C, washed once in cold PBS and the pellets were stored at -80°C until further processing. The samples were suspended in a Laemmli sample buffer and samples corresponding to OD_{600}=0.05 were run on 10% SDS-PAGE gels with 0.5% 2,2,2-trichloroethanol [66]. The gels were then activated for 5 min by 300 nm irradiation on ChemiDoc Imaging System (Bio-Rad) and then the proteins were transferred on 0.4 µm PVDF membrane in Tris-Glycine buffer with 20% methanol for 90 min at 350 mA with cooling. The membranes were then blocked in 3% BSA in TBST buffer for 1 h in room temperature with agitation followed by overnight incubation with 1:2500 mouse anti-GroEL antibody (Thermo Fisher Scientific) and 1:10 000 rabbit anti-enolase (a gift from prof. Ben Luisi) in 3% BSA in TBST overnight at 4 °C. The following day the membranes were washed 3 times in TBST and incubated with 1:10 000 anti-mouse Alexa Fluor 647 and 1:10 000 anti-rabbit Alexa Fluor 488 antibodies (Thermo Fisher Scientific) in 3% BSA in TBST for 1 h at room temperature. The blots were then scanned using the ChemiDoc Imaging System (Bio-Rad) and band intensities were quantified in Image Lab Software (Bio-Rad).

Mass spectrometry proteomic measurement with isobaric labeling (TMT-MS)

Overnight cultures of *E. coli* BW25113 strain transformed with pBAD plasmids encoding degraders and control peptides were grown in LB medium with Ampicillin (100 µg/ml). The cultures were then diluted 1:100 in 10 ml of fresh LB with Ampicillin and grown in 37 °C to OD_{600} 0.1-0.2. The cultures were then induced with 0.02% L-arabinose and grown for 6 h at 42 °C with shaking. The cultures were then centrifuged for 10 min at 1 000 x g at 4 °C, washed once in cold PBS and the pellets were stored at -80 °C until further processing.

Proteins from bacterial pellets were extracted using the Sample Preparation by Easy Extraction and Digestion (SPEED) protocol [67]. In brief, bacterial pellets were solubilized in concentrated TFA (cell pellet/TFA 1:2-1:4 (v/v)) and incubated for 2-10 minutes at RT. Samples were neutralized by adding 2 M Tris-Base buffer using 10×volume of TFA and further incubated at 95°C for 5 min after adding Tris(2-carboxyethyl)phosphine (TCEP) to a final concentration of 10 mM and 2-Chloroacetamide (CAA) to a final concentration of 40 mM. Protein concentrations were determined by turbidity measurements at 360 nm, adjusted to the same concentration using a sample dilution buffer (2 M Tris Base/TFA 10:1 (v/v)) and then diluted 1:4-1:5 with water. Digestion was carried out overnight at 37 °C using trypsin (sequencing grade, Promega) at a protein/enzyme ratio of 100:1. TFA was added to a final concentration of 2% to stop digestion. The resulting peptides were labeled using an on-column TMT labeling protocol [68]. TMT-labeled samples were compiled into a single TMT sample and concentrated using a SpeedVac concentrator. Peptides in the compiled sample were fractionated (6 or 8 fractions) using the bRP fractionation. Prior to LC-MS measurement, the peptide fractions were resuspended in 0.1% TFA, 2% acetonitrile in water.

Chromatographic separation was performed on an Easy-Spray Acclaim PepMap column 50 cm long × 75 µm inner diameter (Thermo Fisher Scientific) at 55 °C by applying 90-120 min acetonitrile gradients in 0.1% aqueous formic acid at a flow rate of 300 nl/min. An UltiMate 3000 nano-LC system was coupled to a Q Exactive HF-X mass spectrometer via an easy-spray source (all Thermo Fisher Scientific). The Q Exactive HF-X was operated in TMT mode with survey scans acquired at a resolution of 60,000 at m/z 200. Up to 15 of the most abundant isotope patterns with charges 2-5 from the survey scan were selected with an isolation window of 0.7 m/z and fragmented by higher-energy collision dissociation (HCD) with normalized collision energies of 32, while the dynamic exclusion was set to 30 or 45 s. The maximum ion injection times for the survey scan and the MS/MS scans (acquired with a resolution of 45,000

at m/z 200) were 50 and 96 or 150 ms, respectively. The ion target value for MS was set to 3e6 and for MS/MS to 1e5, and the minimum AGC target was set to 1 or 2e3.

The data were processed with MaxQuant v. 1.6.17.0 [69], and the peptides were identified from the MS/MS spectra searched against Uniprot *E.coli* Reference Proteome (UP000000625) supplemented with sequences of GroTAC and control peptides using the built-in Andromeda search engine. Reporter ion MS2-based quantification was applied with reporter mass tolerance = 0.003 Da and min. reporter PIF = 0.75. Cysteine carbamidomethylation was set as a fixed modification and methionine oxidation as well as glutamine/asparagine deamination were set as variable modifications. For *in silico* digests of the reference proteome, cleavages of arginine or lysine followed by any amino acid were allowed (trypsin/P), and up to two missed cleavages were allowed. The FDR was set to 0.01 for peptides, proteins and sites. Match between runs was enabled. Other parameters were used as pre-set in the software.

Protein Groups table was loaded into Perseus v.1.6.10.0 [70]. Standard filtering steps were applied to clean up the dataset: reverse (matched to decoy database), only identified by site, and potential contaminants (from a list of commonly occurring contaminants included in MaxQuant) protein groups were removed. Reporter intensity corrected values were log2 transformed and protein groups with all 15 values in a given sample set were kept. The intensity values were then normalized by median subtraction within TMT channels. Student T-testing (permutation-based FDR = 0.01, S0 = 0.2) was performed on the dataset to return protein groups, which levels were statistically significantly changed between groups of samples. The results are provided in a Supplementary Table S5.

This dataset has been deposited to the ProteomeXchange Consortium via the PRIDE partner repository with the dataset identifier PXD045730 [71–73].

ATPase activity assay

The ATPase activity assay was performed as described before [33] using an NADH-coupled assay [74]. The assay was performed in a 96-well plate and carried out in a buffer containing 50 mM Tris (pH 7.5), 200 mM NaCl and 5 mM $MgCl_2$ in the presence of 1-2 mM NADH, 2.5 mM ATP, 2.5 mM phosphoenolpyruvate, 50 µg/ml pyruvate kinase, and 50 µg/ml lactate dehydrogenase. The ClpX interactors (SspB or researched peptides) were added in the appropriate concentrations, and the reaction was started by adding 0.08 µM of $ClpX_6$ to the final volume of 100 µl. Changes in NADH concentration were measured via changes in the absorbance at 340 nm at 30 °C. The absorbance was monitored for 1.5-2 h at 1 min intervals in a Tecan Infinite 200 Pro plate reader (Tecan Group Ltd.). The rate of ATP hydrolysis was calculated assuming a 1:1 ratio between ATP regeneration and NADH oxidation and a Δε340 of 6.23 µM-1cm-1. Within each run the values corresponding to the same interactor concentration were averaged and treated as a technical replicate. Curve fitting and statistical analysis was performed via Graphpad Prism 9 software (Graphpad Software, LLC). The error bars representing SEM are plotted for the points with more than one technical replicate.

SDS-PAGE analysis of *in vitro* degradation

SDS-PAGE analysis of in vitro GroEL degradation by ClpXP was performed as described previously [33]. Reactions were performed in a buffer containing 50 mM Tris (pH 7.5), 200 mM NaCl, 10 mM KCl, and 10 mM $MgCl_2$ in the presence of 2.5 mM ATP, 2.5 mM phosphoenolpyruvate, and 50 µg/ml pyruvate kinase. GroEL or control protein was added to the buffer in the concentration 0.05 - 0.1 µM of $GroEL_{14}$ incubated in RT with or without the presence of 35 µM peptide (XB-GGS, XB-GGS-SBP, or GGS-SBP). After 10 min, 0.8 µM of $ClpX_6$ was added, and the samples were further incubated for 15 min in RT. The reaction was started by adding 2.1 µM of $ClpP_{14}$ to the final volume of 100 µl and performed at 30 °C. 10 µl samples were collected in 2 h intervals up to 10 h. The degradation reaction was stopped by

adding the Laemmli loading buffer followed by 5 min incubation at 95°C. Prepared samples were applied on 8-10% SDS-PAGE gels, resolved at 200 V and visualized using SafeStain dye. The band intensities were measured in Image Lab Software (Bio-Rad). The intensities of bands corresponding to GroEL were normalized to the intensities of the pyruvate kinase bands. The relative intensity at 0 h was treated as 100% and the rest of the points were compared to the point at 0 h.

Characterization of peptide-protein interactions by biolayer interferometry

The interactions of peptides (GroTAC, XB-GGS, GGS-SBP) with ClpX and GroEL were characterized by biolayer interferometry using Octet R2 (Sartorius) and Octet NTA Biosensors. The optimal protein and peptide concentrations were determined separately for each of the proteins by performing ligand scout experiments at fixed protein concentration and different ligand concentrations including sensors without ligands as binding specificity control. The optimal ligand concentrations were determined by loading scout experiments (Fig. S8 A-D). The interactions between ClpX and the peptides were measured at 30 °C in the buffer containing 25 mM HEPES (pH 8.0), 200 mM KCl, 10 mM $MgCl_2$, 0.5 % Tween-20, and 2.5 mM ATP. The sensors were loaded with 150 nM of His-SUMO-XB-GGS or 100 nM of HisSUMO-XB-GGS-SBP, followed by blocking with 86 nM HisSUMO. The binding kinetics was then determined by measuring the interaction with a two-fold dilution series of ClpX in concentrations from 1 µM to 31.25 nM. A control without ClpX was included in the assay. The interaction with GroEL was measured at 30 °C in the buffer containing 25 mM HEPES (pH 8.0), 300 mM KCl, 10 mM $MgCl_2$, 0.5 % Tween-20, and 12.5 mM ATP. The sensors were loaded with 200 nM HisSUMO-GGS-SBP or 400 nM HisSUMO-XB-GGS-SBP and blocked with 257 nM HisSUMO. The concentration range of GroEL ranged from 2.5 µM to 78.1 nM with one reference sensor without GroEL. The results were analyzed with the Octet Analysis Studio software (Sartorius), subtracting the signal from the sensor without the analyte and aligning the initial baseline and dissociation steps. The obtained kinetic parameters were obtained assuming the 1:1 binding ratio.

CryoEM structure of the GroEL-GroTAC complex

The complex of GroEL with chemically synthesized XB-PEG3-SBP peptide (KareBay Biochem) was formed by mixing 70 µM $GroEL_{14}$ with 140 µM peptide in the CryoEM buffer (50 mM HEPES pH 8.0, 200 mM KCl, 5 mM $MgCl_2$) and incubating the mixture in room temperature for 20 min. The ATP was added immediately before freezing the sample for the final concentration of 1 mM. 3 µl of the sample mixture was deposited on the glow discharged (25 mA, 0.38 mbar for 50 s) Quantifoil R 2/2 mesh 200 Cu grid. and vitrified in liquid ethane with an FEI Vitrobot Mark IV (Thermo Fisher Scientific) at 4 °C with 100% humidity and 3 s blot time with blotting force 3. The grid was imaged with a Glacios electron microscope (Thermo Fisher Scientific) that operated at 200 kV and was equipped with a Falcon 3EC camera at the Cryomicroscopy and Electron Diffraction Core Facility at the Centre of New Technologies, University of Warsaw. A total of 4672 movies in .mrc format were recorded in a counting mode with a physical pixel size of 0.5878 Å (nominal magnification of 240 000×), 100 µm objective aperture, and nominal defocus range of −2.2 µm to −0.8 µm (with 0.2 µm steps). The total dose (fractionated into 27 frames) was 40 e/Å2, and the dose rate was 0.76 e/pixel/s.

Cryo-EM data processing

Cryo-EM images were processed with cryoSPARC 4.2. Firstly, raw movies were subjected to the cryoSPARC in-built patch motion correction followed by the patch CTF estimation algorithms. A total of 350 383 particles were picked from the whole dataset using a template picker generated by a manual picker. Particles were subjected to four rounds of 2D classification with 250 Å circular mask diameter. A total of 203 031 particles were extracted with box size of 560 px and used to generate de novo a 3D initial model with maximum

resolution set to 12 Å. The generated model was aligned to D7 symmetry axes and 3D refined with imposed D7 symmetry using the homogenous refinement algorithm which resulted in 2.91 Å reconstruction. The model was then used to run a Reference Based Motion Correction in cryoSPARC 4.4. The resulting particles were used for a new Ab-Initio model followed by homogenous refinement with imposed D7 symmetry, as well as local and global CTF refinements and the Ewald sphere correction with negative curvature sign, which produced a map with a resolution of 2.45 Å. The obtained map was deposited in EMDB (ID EMD-19687)

Model building in cryo-EM maps

The obtained Cryo-EM maps were processed using a few standard modelling protocols for building models from Cryo-EM data. A portion of GroEL was usually reconstructed in agreement with available structures in the PDB database; however, due to the lower resolution of the peptide fragments, the interacting peptides were not reconstructed. Therefore, we employed the newly published ModelAngelo method, which automates atomic modelling in Cryo-EM maps and constructs protein models of comparable quality to those built by human experts [75]. ModelAngelo utilizes machine learning to model building in three steps: (1) prediction of residues (Cα atoms positions) based on cryo-EM map, (2) optimization of residue positions and orientations, creating a graph of connections, (3) generating of a full-atom model.

In many GroEL regions, especially near GroEL-GroTAC interface and in the flexible loops on the outside of the barrel, the map had much lower resolution. Consequently, the neural network predicted different residues than the input sequence of GroEL, which were then removed from the final structure in the 3rd stage of ModelAngelo refinement. Therefore, we decided to use the model from the previous step (in Cα representation) for further processing. Gaps (errors) in the identification of GroEL residues were manually corrected. Based on available PDB structures (PDB ID 1MNF) we changed the identity of misidentified residues. Prediction of peptide fragments was not straightforward due to the low resolution of the cryoEM map in this region. In the expected peptide region, ModelAngelo identified usually from 7 to 10 Cα positions (which is much fewer than the 13 residues from the XB peptide, the $(PEG)_3$ linker, and the 12 residues of SBP). In most cases, predicted residues differed significantly from the peptide sequence. One of the only consistently recognized residues was proline at one of the Cα positions. When we superimposed the ModelAngelo structure on the PDB structure (PDB ID 1MNF), this Cα position was near the P6 Cα position from SBP. Therefore, without any other leads, we assigned identities to the Cα positions in ModelAngelo structure, that were close in the superimposed PDB structure. The comparison between our final model and PDB model can be seen in Figure S9. Finally, the obtained Cα resolution model was reconstructed into a full-atom representation using cg2all method guided by cryoEM data. Cg2all has been demonstrated to be a useful tool in the accurate refinement of all-atom coordinates against intermediate- and low-resolution cryo-EM densities [76]. This model was then used for refinement against the map. The first stage of refinement was done in Coot [77]. The final refinement stage involved two rounds of Real Space Refine in Phenix [78]. After final corrections, the obtained model was validated and deposited to PDB database (PDB ID 8S32).

Author contributions

Conceptualization, M.A.I.N, M.M.K., and M.W.G.; Methodology, M.A.I.N., M.M.K., A.A. and M.W.G.; Data acquisition, M.A.I.N., M.M.K., A.A., K.J.B, T.K.G, and R.A.S.; Data analysis and interpretation, M.A.I.N., M.M.K., A.A., K.W., T.K.G, R.A.S, and M.W.G.; writing—original draft preparation, M.A.I.N. and M.W.G.; writing - review and editing, M.M.K. and R.A.S.; supervision and funding acquisition, S.K. and M.W.G.

Acknowledgements

The authors thank Agata Krawczyk-Balska, Ben Luisi and Paulina Dominiak for helpful discussions. This work was funded by grant number POIR.04.04.00-00-5EC1/18-00 to MG for the project “Proteolysis-targeting strategies in bacterial systems for functional studies of proteins and improvement of antibiotics” carried out within the FIRST TEAM programme of the Foundation for Polish Science co-financed by the European Union under the European Regional Development Fund. KW and SK acknowledge funding from the National Science Centre, Poland [2020/39/B/NZ2/01301]. CryoEM data collection was enabled by the Ministry of Science and Higher Education programme “Excellence Initiative – Research University (2020-2026) (IDUB)” awarded to the University of Warsaw, in particular, the 1.4.1. Activity “Strengthening the core-facility potential on the Ochota Campus” and grant BOB-IDUB-622-20/2021 entitled “Infrastructure for Cryomicroscopy and Electron Diffraction Core Facility” & I.4.2. Fund for the Renovation and Development of Research Infrastructure – development and maintenance of infrastructure.

Conflict of interest

M.W.G., M.A.I.N., M.M.K. and A.A. are holders of a patent application related to this work (P.439032, PCT/IB2022/059128)

Bibliography

1. Varshavsky A. Naming a targeting signal. *Cell*. 1991;64(1):13-15. doi:10.1016/0092-8674(91)90202-A
2. Izert MA, Klimecka MM, Górna MW. Applications of Bacterial Degrons and Degraders — Toward Targeted Protein Degradation in Bacteria. *Frontiers in Molecular Biosciences*. 2021;8(May):1-21. doi:10.3389/fmolb.2021.669762
3. Wei JR, Krishnamoorthy V, Murphy K, et al. Depletion of antibiotic targets has widely varying effects on growth. *Proceedings of the National Academy of Sciences of the United States of America*. 2011;108(10):4176-4181. doi:10.1073/pnas.1018301108
4. Potvin-Trottier L, Lord ND, Vinnicombe G, Paulsson J. Synchronous long-term oscillations in a synthetic gene circuit. *Nature*. 2016;538(7626):514-517. doi:10.1038/nature19841
5. Durante-Rodríguez G, De Lorenzo V, Nikel PI. A Post-translational Metabolic Switch Enables Complete Decoupling of Bacterial Growth from Biopolymer Production in Engineered Escherichia coli. *ACS Synthetic Biology*. 2018;7(11):2686-2697. doi:10.1021/acssynbio.8b00345
6. Lei Y, Chen W, Xiang L, et al. Engineering an SspB-mediated degron for novel controllable protein degradation. *Metabolic Engineering*. 2022;74(June):150-159. doi:10.1016/j.ymben.2022.10.013
7. Gopal P, Sarathy JP, Yee M, et al. Pyrazinamide triggers degradation of its target aspartate decarboxylase. *Nature Communications*. 2020;11(1):1-10. doi:10.1038/s41467-020-15516-1
8. Liu X, Ciulli A. Proximity-Based Modalities for Biology and Medicine. *ACS Central Science*. 2023;9(7):1269-1284. doi:10.1021/acscentsci.3c00395
9. Sakamoto KM, Kim KB, Kumagai A, Mercurio F, Crews CM, Deshaies RJ. Protacs: Chimeric molecules that target proteins to the Skp1–Cullin–F box complex for ubiquitination and degradation. *Proceedings of the National Academy of Sciences*. 2001;98(15):8554-8559. doi:10.1073/pnas.141230798
10. Takahashi D, Moriyama J, Nakamura T, et al. AUTACs: Cargo-Specific Degraders Using Selective Autophagy. *Molecular Cell*. 2019;76(5):797-810.e10. doi:10.1016/j.molcel.2019.09.009
11. Banik SM, Pedram K, Wisnovsky S, Ahn G, Riley NM, Bertozzi CR. Lysosome-targeting chimaeras for degradation of extracellular proteins. *Nature*. 2020;584(7820):291-297. doi:10.1038/s41586-020-2545-9

12. Cotton AD, Nguyen DP, Gramespacher JA, Seiple IB, Wells JA. Development of Antibody-Based PROTACs for the Degradation of the Cell-Surface Immune Checkpoint Protein PD-L1. *Journal of the American Chemical Society*. 2021;143(2):593-598. doi:10.1021/jacs.0c10008
13. Mayor-Ruiz C, Bauer S, Brand M, et al. Rational discovery of molecular glue degraders via scalable chemical profiling. *Nature Chemical Biology*. 2020;16(11):1199-1207. doi:10.1038/s41589-020-0594-x
14. Słabicki M, Kozicka Z, Petzold G, et al. The CDK inhibitor CR8 acts as a molecular glue degrader that depletes cyclin K. *Nature*. 2020;585(7824):293-297. doi:10.1038/s41586-020-2374-x
15. Chirnomas D, Hornberger KR, Crews CM. Protein degraders enter the clinic — a new approach to cancer therapy. *Nature Reviews Clinical Oncology*. Published online February 13, 2023. doi:10.1038/s41571-023-00736-3
16. Samarasinghe KTG, An E, Genuth MA, Chu L, Holley SA, Crews CM. OligoTRAFTACs: A generalizable method for transcription factor degradation. *RSC Chemical Biology*. 2022;3(9):1144-1153. doi:10.1039/D2CB00138A
17. Wang S, Han L, Han J, et al. Uncoupling of PARP1 trapping and inhibition using selective PARP1 degradation. *Nature Chemical Biology*. 2019;15(12):1223-1231. doi:10.1038/s41589-019-0379-2
18. Kim C, Wang XD, Liu Z, Zha S, Yu Y. Targeting Scaffolding Functions of Enzymes Using PROTAC Approaches. *Biochemistry*. 2023;62(3):561-563. doi:10.1021/acs.biochem.2c00366
19. Bondeson DP, Mares A, Smith IED, et al. Catalytic in vivo protein knockdown by small-molecule PROTACs. *Nat Chem Biol*. 2015;11(8):611-617. doi:10.1038/nchembio.1858
20. de Wispelaere M, Du G, Donovan KA, et al. Small molecule degraders of the hepatitis C virus protease reduce susceptibility to resistance mutations. *Nat Commun*. 2019;10(1). doi:10.1038/s41467-019-11429-w
21. Hughes SJ, Testa A, Thompson N, Churcher I. The rise and rise of protein degradation: Opportunities and challenges ahead. *Drug Discov Today*. 2021;26(12):2889-2897. doi:10.1016/j.drudis.2021.08.006
22. Bashore C, Prakash S, Johnson MC, et al. Targeted degradation via direct 26S proteasome recruitment. *Nature Chemical Biology 2022 19:1*. 2022;19(1):55-63. doi:10.1038/s41589-022-01218-w
23. Morreale FE, Kleine S, Leodolter J, et al. BacPROTACs mediate targeted protein degradation in bacteria. *Cell*. 2022;185(13):2338-2353.e18. doi:10.1016/j.cell.2022.05.009
24. Flynn JM, Neher SB, Kim YI, Sauer RT, Baker TA. Proteomic discovery of cellular substrates of the ClpXP protease reveals five classes of ClpX-recognition signals. *Molecular Cell*. 2003;11(3):671-683. doi:10.1016/S1097-2765(03)00060-1
25. Gottesman S, Roche E, Zhou YN, Sauer RT. The ClpXP and ClpAP proteases degrade proteins with carboxy-terminal peptide tails added by the SsrA-tagging system. *Genes and Development*. 1998;12(9):1338-1347. doi:10.1101/gad.12.9.1338
26. Kim JH, Wei JR, Wallach JB, Robbins RS, Rubin EJ, Schnappinger D. Protein inactivation in mycobacteria by controlled proteolysis and its application to deplete the beta subunit of RNA polymerase. *Nucleic Acids Research*. 2011;39(6):2210-2220. doi:10.1093/nar/gkq1149
27. Griffith KL, Grossman AD. Inducible protein degradation in Bacillus subtilis using heterologous peptide tags and adaptor proteins to target substrates to the protease ClpXP. *Molecular Microbiology*. 2008;70(4):1012-1025. doi:10.1111/j.1365-2958.2008.06467.x
28. Davis JH, Baker TA, Sauer RT. Engineering Synthetic Adaptors and Substrates for Controlled ClpXP Degradation. *Journal of Biological Chemistry*. 2009;284(33):21848-21855. doi:10.1074/jbc.M109.017624

29. Davis JH, Baker TA, Sauer RT. Small-molecule control of protein degradation using split adaptors. *ACS Chemical Biology*. 2011;6(11):1205-1213. doi:10.1021/cb2001389
30. Ghanbarpour A, Fei X, Baker TA, Davis JH, Sauer RT. The SspB adaptor drives structural changes in the AAA+ ClpXP protease during ssrA-tagged substrate delivery. *Proceedings of the National Academy of Sciences*. 2023;120(6):2017. doi:10.1073/pnas.2219044120
31. Park EY, Lee BG, Hong SB, Kim HW, Jeon H, Song HK. Structural Basis of SspB-tail Recognition by the Zinc Binding Domain of ClpX. *Journal of Molecular Biology*. 2007;367(2):514-526. doi:10.1016/j.jmb.2007.01.003
32. Song HK, Eck MJ. Structural basis of degradation signal recognition by SspB, a specificity-enhancing factor for the ClpXP proteolytic machine. *Molecular Cell*. 2003;12(1):75-86. doi:10.1016/S1097-2765(03)00271-5
33. Klimecka MM, Antosiewicz A, Izert MA, et al. A Uniform Benchmark for Testing SsrA-Derived Degrons in the Escherichia coli ClpXP Degradation Pathway. *Molecules*. 2021;26(19):5936. doi:10.3390/molecules26195936
34. Dougan DA, Weber-Ban E, Bukau B. Targeted Delivery of an ssrA-Tagged Substrate by the Adaptor Protein SspB to Its Cognate AAA+ Protein ClpX. *Molecular Cell*. 2003;12(2):373-380. doi:10.1016/j.molcel.2003.08.012
35. Kim YI, Levchenko I, Fraczkowska K, Woodruff R V., Sauer RT, Baker TA. Molecular determinants of complex formation between Clp/Hsp 100 ATPases and the ClpP peptidase. *Nature Structural Biology*. 2001;8(3):230-233. doi:10.1038/84967
36. Lee HM, Ren J, Tran KM, et al. Identification of efficient prokaryotic cell-penetrating peptides with applications in bacterial biotechnology. *Communications Biology*. 2021;4(1):205. doi:10.1038/s42003-021-01726-w
37. Oikawa K, Islam MM, Horii Y, Yoshizumi T, Numata K. Screening of a Cell-Penetrating Peptide Library in Escherichia coli: Relationship between Cell Penetration Efficiency and Cytotoxicity. *ACS Omega*. 2018;3(12):16489-16499. doi:10.1021/acsomega.8b02348
38. Kerner MJ, Naylor DJ, Ishihama Y, et al. Proteome-wide analysis of chaperonin-dependent protein folding in Escherichia coli. *Cell*. 2005;122(2):209-220. doi:10.1016/j.cell.2005.05.028
39. Fujiwara K, Ishihama Y, Nakahigashi K, Soga T, Taguchi H. A systematic survey of in vivo obligate chaperonin-dependent substrates. *EMBO Journal*. 2010;29(9):1552-1564. doi:10.1038/emboj.2010.52
40. Niwa T, Fujiwara K, Taguchi H. Identification of novel in vivo obligate GroEL/ES substrates based on data from a cell-free proteomics approach. *FEBS Letters*. 2016;590(2):251-257. doi:10.1002/1873-3468.12036
41. Abdeen S, Salim N, Mammadova N, et al. GroEL/ES inhibitors as potential antibiotics. *Bioorganic and Medicinal Chemistry Letters*. 2016;26(13):3127-3134. doi:10.1016/j.bmcl.2016.04.089
42. Kunkle T, Abdeen S, Salim N, et al. Hydroxybiphenylamide GroEL/ES Inhibitors Are Potent Antibacterials against Planktonic and Biofilm Forms of Staphylococcus aureus. *Journal of Medicinal Chemistry*. 2018;61(23):10651-10664. doi:10.1021/acs.jmedchem.8b01293
43. Chen L, Sigler PB. The Crystal Structure of a GroEL/Peptide Complex. *Cell*. 1999;99(7):757-768. doi:10.1016/S0092-8674(00)81673-6
44. Gragerov A, Zeng L, Zhao X, Burkholder W, Gottesman ME. Specificity of DnaK-peptide binding. *Journal of Molecular Biology*. 1994;235(3):848-854. doi:10.1006/jmbi.1994.1043
45. Otvos L, Insug O, Rogers ME, et al. Interaction between heat shock proteins and antimicrobial peptides. *Biochemistry*. 2000;39(46):14150-14159. doi:10.1021/bi0012843
46. Guzman LM, Belin D, Carson MJ, Beckwith J. Tight regulation, modulation, and high-level expression by vectors containing the arabinose PBAD promoter. *Journal of Bacteriology*. 1995;177(14):4121-4130. doi:10.1128/jb.177.14.4121-4130.1995

47. Martinez-Hackert E, Hendrickson WA. Promiscuous Substrate Recognition in Folding and Assembly Activities of the Trigger Factor Chaperone. *Cell*. 2009;138(5):923-934. doi:10.1016/j.cell.2009.07.044
48. McGinness KE, Baker TA, Sauer RT. Engineering Controllable Protein Degradation. *Molecular Cell*. 2006;22(5):701-707. doi:10.1016/j.molcel.2006.04.027
49. Swulius MT, Jensen GJ. The helical mreb cytoskeleton in Escherichia coli MC1000/pLE7 is an artifact of the N-terminal yellow fluorescent protein tag. *Journal of Bacteriology*. 2012;194(23):6382-6386. doi:10.1128/JB.00505-12
50. Weill U, Krieger G, Avihou Z, Milo R, Schuldiner M, Davidi D. Assessment of GFP Tag Position on Protein Localization and Growth Fitness in Yeast. *Journal of Molecular Biology*. 2019;431(3):636-641. doi:10.1016/j.jmb.2018.12.004
51. Singh M, Sori H, Ahuja R, Meena J, Sehgal D, Panda AK. Effect of N-terminal poly histidine-tag on immunogenicity of Streptococcus pneumoniae surface protein SP0845. *International Journal of Biological Macromolecules*. 2020;163:1240-1248. doi:10.1016/j.ijbiomac.2020.07.056
52. Hoi DM, Junker S, Junk L, et al. Clp-targeting BacPROTACs impair mycobacterial proteostasis and survival. *Cell*. 2023;186(10):2176-2192.e22. doi:10.1016/j.cell.2023.04.009
53. Ikuta KS, Swetschinski LR, Robles Aguilar G, et al. Global mortality associated with 33 bacterial pathogens in 2019: a systematic analysis for the Global Burden of Disease Study 2019. *The Lancet*. 2022;0(0). doi:10.1016/S0140-6736(22)02185-7
54. Lorimer GH. A quantitative assessment of the role of the chaperonin proteins in protein folding in vivo. *The FASEB Journal*. 1996;10(1):5-9. doi:10.1096/fasebj.10.1.8566548
55. Farrell CM, Grossman AD, Sauer RT. Cytoplasmic degradation of ssrA-tagged proteins. *Molecular Microbiology*. 2005;57(6):1750-1761. doi:10.1111/j.1365-2958.2005.04798.x
56. Li GW, Burkhardt D, Gross C, Weissman JS. Quantifying absolute protein synthesis rates reveals principles underlying allocation of cellular resources. *Cell*. 2014;157(3):624-635. doi:10.1016/J.CELL.2014.02.033
57. Walker TE, Shirzadeh M, Sun HM, et al. Temperature Regulates Stability, Ligand Binding (Mg2+and ATP), and Stoichiometry of GroEL-GroES Complexes. *Journal of the American Chemical Society*. 2022;144(6):2667-2678. doi:10.1021/jacs.1c11341
58. Martin J, Horwich AL, Hartl FU. Prevention of Protein Denaturation Under Heat Stress by the Chaperonin Hsp60. *Science*. 1992;258(5084):995-998. doi:10.1126/science.1359644
59. Pla-Prats C, Cavadini S, Kempf G, Thomä NH. Recognition of the CCT5 di-Glu degron by CRL4DCAF12 is dependent on TRiC assembly. *The EMBO Journal*. 2023;42(4):e112253. doi:10.15252/EMBJ.2022112253
60. Yagita Y, Zavodszky E, Peak-Chew SY, Hegde RS. Mechanism of orphan subunit recognition during assembly quality control. *Cell*. Published online July 21, 2023. doi:10.1016/J.CELL.2023.06.016
61. Schneider M, Radoux CJ, Hercules A, et al. The PROTACtable genome. *Nature Reviews Drug Discovery*. 2021;20(10):789-797. doi:10.1038/s41573-021-00245-x
62. Chai Q, Wang Z, Webb SR, Dutch RE, Wei Y. The ssrA-Tag Facilitated Degradation of an Integral Membrane Protein. *Biochemistry*. 2016;55(16):2301-2304. doi:10.1021/acs.biochem.6b00038
63. Moore SD, Baker TA, Sauer RT. Forced extraction of targeted components from complex macromolecular assemblies. *Proceedings of the National Academy of Sciences of the United States of America*. 2008;105(33):11685-11690. doi:10.1073/pnas.0805633105
64. Abeywansha T, Chai Q, Zhang X, Wang Z, Wei Y. Accessibility from the Cytoplasm Is Critical for ssrA Tag-Mediated Degradation of Integral Membrane Proteins by ClpXP Protease. *Biochemistry*. 2018;57(38):5602-5608. doi:10.1021/acs.biochem.8b00641

65. Baba T, Ara T, Hasegawa M, et al. Construction of Escherichia coli K-12 in-frame, single-gene knockout mutants: the Keio collection. *Mol Syst Biol*. 2006;2(1). doi:10.1038/msb4100050
66. Ladner CL, Yang J, Turner RJ, Edwards RA. Visible fluorescent detection of proteins in polyacrylamide gels without staining. *Analytical Biochemistry*. 2004;326(1):13-20. doi:10.1016/j.ab.2003.10.047
67. Doellinger J, Schneider A, Hoeller M, Lasch P. Sample preparation by easy extraction and digestion (SPEED) - A universal, rapid, and detergent-free protocol for proteomics based on acid extraction. *Molecular and Cellular Proteomics*. 2020;19(1):209-222. doi:10.1074/mcp.TIR119.001616
68. Myers SA, Rhoads A, Cocco AR, et al. Streamlined Protocol for Deep Proteomic Profiling of FAC-sorted Cells and Its Application to Freshly Isolated Murine Immune Cells*. *Molecular & Cellular Proteomics*. 2019;18(5):995-1009. doi:10.1074/mcp.RA118.001259
69. Tyanova S, Temu T, Cox J. The MaxQuant computational platform for mass spectrometry-based shotgun proteomics. *Nature Protocols*. 2016;11(12):2301-2319. doi:10.1038/nprot.2016.136
70. Tyanova S, Temu T, Sinitcyn P, et al. The Perseus computational platform for comprehensive analysis of (prote)omics data. *Nature Methods*. 2016;13(9):731-740. doi:10.1038/nmeth.3901
71. Perez-Riverol Y, Xu QW, Wang R, et al. PRIDE inspector toolsuite: Moving toward a universal visualization tool for proteomics data standard formats and quality assessment of proteomexchange datasets. *Molecular and Cellular Proteomics*. 2016;15(1):305-317. doi:10.1074/mcp.O115.050229
72. Perez-Riverol Y, Bai J, Bandla C, et al. The PRIDE database resources in 2022: A hub for mass spectrometry-based proteomics evidences. *Nucleic Acids Research*. 2022;50(D1):D543-D552. doi:10.1093/nar/gkab1038
73. Deutsch EW, Bandeira N, Perez-Riverol Y, et al. The ProteomeXchange consortium at 10 years: 2023 update. *Nucleic Acids Research*. 2023;51(D1):D1539-D1548. doi:10.1093/nar/gkac1040
74. JG N. Coupled assay of Na+,K+-ATPase activity. *Methods in enzymology*. 1988;156(C):116-119. doi:10.1016/0076-6879(88)56014-7
75. Jamali K, Käll L, Zhang R, Brown A, Kimanius D, Scheres SHW. Automated model building and protein identification in cryo-EM maps. *Nature*. Published online February 26, 2024. doi:10.1038/s41586-024-07215-4
76. Heo L, Feig M. One particle per residue is sufficient to describe all-atom protein structures. *bioRxiv*. Published online 2023:2023.05.22.541652. doi:10.1101/2023.05.22.541652
77. Emsley P, Lohkamp B, Scott WG, Cowtan K. Features and development of Coot. *Acta Crystallographica Section D: Biological Crystallography*. 2010;66(4):486-501. doi:10.1107/S0907444910007493
78. Liebschner D, Afonine P V., Baker ML, et al. Macromolecular structure determination using X-rays, neutrons and electrons: Recent developments in Phenix. *Acta Crystallographica Section D: Structural Biology*. 2019;75:861-877. doi:10.1107/S2059798319011471